A STUDY OF CHANGES IN DEFORMATION AND METABOLISM IN LEFT VENTRICLE AS A FUNCTION OF HYPERTROPHY IN SPONTANEOUS HYPERTENSIVE RATS USING MICROPET TECHNOLOGY

Grant T. Gullberg, Ronald H. Huesman, Bryan W. Reutter, Arkadiusz Sitek, Alexander I. Veress, Jeffrey A. Weiss, Yongfeng Yang

This was presented as a poster at the International Conference of Nuclear Cardiology, Lisbon, Portugal, May 8-11, 2005.

Grant T. Gullberg
Life Science Division,
E. O. Lawrence Berkeley National Laboratory
Berkeley, CA 94720
Department of Radiology
University of California San Francisco
San Francisco, CA
gtgullberg@lbl.gov

Ronald H. Huesman
Life Science Division,
E. O. Lawrence Berkeley National Laboratory
Berkeley, CA 94720

Bryan W. Reuter
Life Science Division,
E. O. Lawrence Berkeley National Laboratory
Berkeley, CA 94720

Arkadiusz Sitek
Life Science Division,
E. O. Lawrence Berkeley National Laboratory
Berkeley, CA 94720

Alexander I. Veress
Department of Mechanical Engineering
University of Washington
Stevens Way, Box 35260
Seattle, WA 98195
averess@uw.edu

Jeffrey A. Weiss,
University of Utah
Department of Bioengineering
Salt Lake City, UT 84112
Jeff.weiss@utah.edu

Yongfeng Yang
Department of Biomedical Engineering
University of California
Davis, CA 95616

ABSTRACT

Problem: In the case of hypertrophy caused by pressure overload (hypertension) there is an increase in cardiac mass and modification cardiac metabolism.
Aim: This study was designed to study the changes in glucose metabolism, ejection fraction, and deformation in the left ventricle with the progression of hypertrophy in spontaneous hypertensive rats (SHR).
Methods: Dynamic PET data were acquired using the microPET II at UC Davis. Two rats were imaged at 10-week intervals for 18 months. Each time a dose of approximately 1- 1.5 mCi of F-18-FDG was injected into a normotensive Wistar Kyoto (WKY) rat and the same dose was injected into a SHR rat. Each rat was imaged using a gated dynamic acquisition for 80 minutes acquiring list mode data with cardiac gating of approximately 600-900 million total counts. For the analysis of **glucose of metabolism**, the list mode data were histogrammed into a dynamic sequence (42 frames over 80 mins). For each time frame, projection data of 1203 140×210 sinograms of 0.582 mm bins were formed by summing the last three gates before and one after the R-wave trigger to correspond to the diastolic phase of the cardiac cycle. Dynamic sequences of 128×128×83 matrices of 0.4×0.4×0.582 mm^3 voxels in x, y, and z were reconstructed using an iterative MAP reconstruction which used a prior that penalized the high frequency components of the reconstruction using appropriate weighting between 26 nearest neighboring voxels. Time activity curves were generated from the dynamic reconstructed sequence for the blood and left ventricular tissue regions of interest which were fit to a 2-compartment model to obtain a least squares fit for the kinetic parameters. For the analysis of **deformation**, the list mode data were histogrammed into 8 gates of the cardiac cycle, each gate was the total sum of the later **60 mins** of the **80 min** acquisition. Images of 128×128×83 matrices for each gate were reconstructed using the same iterative MAP reconstruction used to reconstruct the dynamic sequence. The in-plane image dimensions were doubled to 256×256×83 in order to increase the resolution for the Warping analyses. These image data sets were then cropped to 128×128×83. The end-systolic image data sets were designated as the *template* images and the end-diastole image data sets were designated as the *target* images, thus providing an analysis of the diastolic relaxation and filling phases of the cardiac cycle. The template images were manually segmented to create surface definitions representing the epi- and endocardial surfaces. Finite element models of the left ventricles were created using the segmented surfaces and defining a transversely isotropic material with fiber angles varying from the epicardial surface to the endocardial surface. A Warping analyses was performed to obtain the LV strain tensor and fiber stretch distributions.
Results: In one study, the average first principal Green-Lagrange strain, fiber stretch, ejection fraction, and metabolic rate of F-18-FDG was 0.22, 1.08, 80%, **0.1** for the WKY rat and 0.16, 1.06, 50%, **0.25** for the SHR rat, respectively. These same rats studied a year later presented with a metabolic rate of F-18-FDG of 0.11 and 0.25 for the WKY and SHR, respectively. A follow-up study the average strain (n=10) and ejection fraction (n=18) was 0.21, 72.7% for WKY and 0.17, 69.8% for the SHR, respectively.
Conclusion: In the case of pressure overload there is an increased reliance on carbohydrate oxidation in an attempt to maintain contractile function.

INTRODUCTION

In the case of hypertrophy caused by pressure overload (hypertension) there is an increase in cardiac mass and modification of cardiac metabolism. This study was designed to study the changes in glucose metabolism, ejection fraction, and deformation in the left ventricle with the progression of hypertrophy in spontaneous hypertensive rats (SHR).

Deformation. In this study, the left ventricular deformation was quantified by Warping analysis of microPET images of a normotensive Wistar Kyoto (WKY) rat and a spontaneously hypertensive rat (SHR). Regional wall motion analysis in conjunction with global left ventricular ejection fraction are commonly used to assess diastolic function [1]. Nuclear cardiac imaging systems have the capability to evaluate wall motion and wall thickening [2, 3]. While wall motion and wall thickening analyses provide useful measures of local wall function, a more direct measurement of wall contraction/dilation would be the measurement of local deformation (strain) or fiber contraction/extension (stretch). For example, local wall deformation information would be valuable to the clinician in order to evaluate the extent and distribution of diastolic dysfunction due to wall stiffening which may not be apparent in the wall motion and thickening analyses.

Metabolism. Under normal fasting conditions, exogenous fatty acids are the preferred metabolic substrate of the heart, accounting for 60-70% of the energy production [4]. Even though studies show mixed results [5, 6], it is generally felt that the heart switches to a reliance on glycolysis as the primary pathway for energy production during the development of heart failure [7]. In the case of pressure overload there is an increase in cardiac mass, re-expression of fetal genes, a suppression of genes related to several rate-limiting enzymes in fatty acid oxidation, enhancement of genes related to rate-limiting enzyme for glucose oxidation, and increased reliance on carbohydrate oxidation to enable maintenance of contractile function [8,9]. Also, an increased adrenergic tone in the setting of heart failure not only

exerts a direct toxic effect on the myocyte [10] but also causes unfavorable changes in myocardial energy use [11]. With progression of heart failure there is a metabolic remodeling from adaptation to maladaption where regulated metabolic pathways become dysregulated metabolic pathways and the failing heart loses its ability to switch to the most efficient fuel for energy production, thus, becoming an energy-starved heart [4]. In advanced stages of heart failure the myocardial extraction and retention of fatty acid were further impaired [7]. Even though it is not fully understood, it may be that shifts in myocardial glucose and fatty acid use are an important mechanism for the impaired efficiency of the failing heart and a target for specific therapies designed to decrease overall energy requirements.

Figure 1. MicroPET II at UC Davis

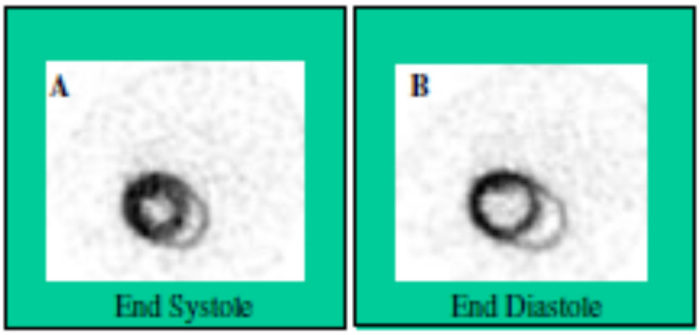

Figure 2. Example slice of the *template* **(A)** end-systolic and *target* **(B)** end-diastolic image data sets of the hypertensive SHR rat from the dynamic acquisition of 06Aug03.

	Type of Acquisition	Blood Pressure (mm Hg)	Birth/ Death	Ratio of Heart to Body Weight
WKY	Dynamic	154[+](07/13/04) 97*(04/19/05)	04/14/03 04/28/05[++]	0.0039
WKY (Blue)	Dynamic	119[+](07/13/04) 105*(04/19/05)	04/14/03 04/28/05[++]	0.0046
SHR	Dynamic	167[+](07/13/04)	04/14/03 02/02/05	
SHR (Red)	Dynamic	165[+](07/13/04)	04/14/03 02/19/05	0.0063

[+] Measurement taken awake, *Measurement taken anesthetized, [++]Death by euthanasia

Table 1. Physiological Factors. Note recirculation time = 8s under anesthesia

METHODS

Dynamic PET data were acquired using the microPET II at UC Davis (Figure 1). Normotensive Wistar Kyoto rats (WKY) and SHR rats were imaged at 10-week intervals. Each time a dose of 1- 2 mCi of F-18-FDG was injected and gated list mode data of 600-900 million counts were acquired over 60-80 mins.

Deformation. List mode data were histogrammed into 8 gates of the cardiac cycle; summing the latter 50 mins of the 80 min acquisition for the dynamic scans and summing all 60 mins for the static acquisitions. Images of 128×128×83 matrices for each gate were reconstructed using the same iterative MAP reconstruction used to reconstruct the dynamic sequence. These image data sets were then cropped to 128×128×35. The end-systolic image data sets were manually segmented creating epi- and endocardial surfaces of the LV. The end-systolic image data sets were designated as the template images

and the end-diastolic image data sets were designated as the target images (Figure 2), thus providing an analysis of the diastolic relaxation and filling phases of the cardiac cycle. Finite element models of the left ventricles were created in NIKE3D [12] using the segmented surfaces and defining a transversely isotropic material [13] with realistic fiber angle distributions varying from the epicardial surface to the endocardial surface [14, 15]. The material coefficients of the model were determined by a nonlinear least squares fit of the transversely isotropic material of the equibiaxial stress/strain curves presented in [15] for the WKY rat left ventricle.

Hyperelastic Warping [16, 17] was performed on these images to obtain a fit to the end-diastolic image data sets providing an analysis of diastolic relaxation (LV strain tensor and fiber stretch distributions). In Warping, a spatial discretization of the template image is deformed into alignment with the target image. An image energy is defined as the difference in image intensities. The Warping analyses provided the LV first principal Green-Lagrange strain and fiber stretch (extended length/reference length) distributions documented in the normotensive WKY and spontaneously hypertensive rat (SHR) image data sets. The 1st principal Green-Lagrange strain is the maximum of the three eigenvalues of the strain tensor, and represents the magnitude of the largest local tensile strain along the principal direction.

Glucose metabolism. List mode microPET data were histogrammed into 8 gates of the cardiac cycle. For each gate the dynamic sequence consisted of complete tomographic projections formed at 12 intervals of 5s, followed by 6 of 10s, 4 of 30s, 6 of 60s, and finally 14 intervals of 300s to give a total of 42 time frames over the 80 mins. For each interval, projection data of 1203 140×210 sinograms of 0.582 mm bins were formed by summing the last three gates before and one after the R-wave trigger to correspond to the diastolic phase of the cardiac cycle. Since randoms were pre-subtracted from the prompts, a shifted Poisson likelihood function was used to model the random subtraction [18].

Dynamic sequences of 128×128×83 matrices of 0.4 ×0.4 ×0.582 mm3 voxels in x, y, and z were reconstructed using an iterative MAP reconstruction [19]. The MAP algorithm scales the weighting of the prior to keep the resolution constant throughout the image. The projector and backprojector used a factor system matrix [19] that modeled the solid angle effect, crystal penetration, intercrystal scatters, and the block structure of the microPET II. The prior penalized the high frequency components of the reconstruction using appropriate weighting between 26 nearest neighboring voxels. The weighing of the prior was scaled so that the weighting between the prior and the likelihood function remained relatively the same from time frame to time frame as the counts change in the data due to the wash-in and wash-out of FDG from the myocardium.

A blood (~100 mm3) and left ventricle tissue (~320 mm3) volumes of interest were determined from a reconstruction of the last 50 mins of the acquisition. Time activity curves were generated from the dynamic reconstructed sequence for the blood region and left ventricular tissue region and compared with curves generated using factor analysis of dynamic structures (FADS) [20]. The dynamic data generated from the myocardial tissue and blood regions of interest were fit to a 2-compartment model (Figure 3) using RFIT [21] to obtain a weighted least squares fit for the kinetic parameters.

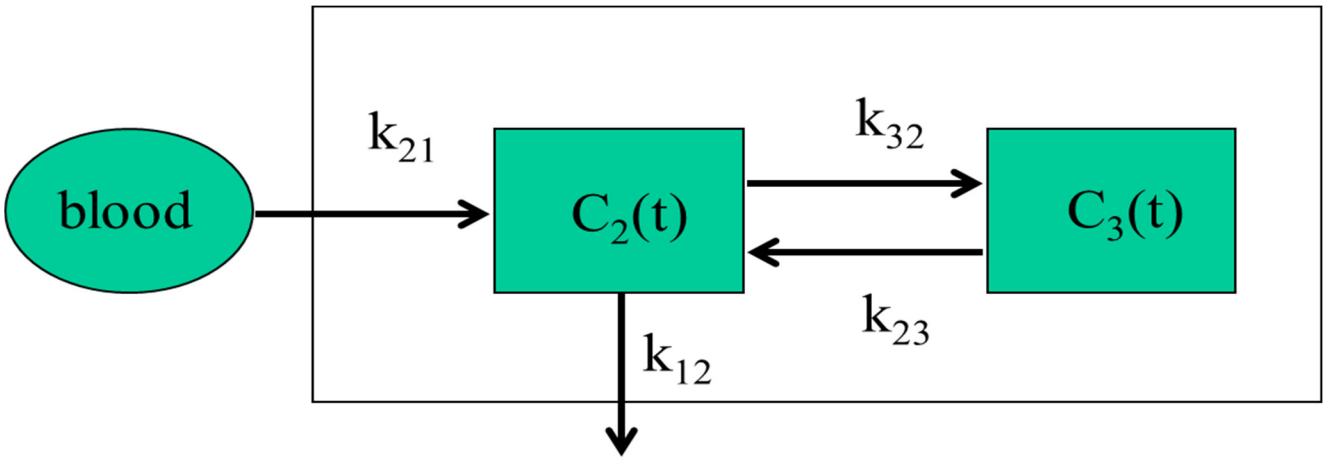

Figure 3. FDG Compartment Model. $C_2(t)$ – FDG in the extravascular space and $C_3(t)$ – FDG-6-P in cells.

RESULTS

Deformation

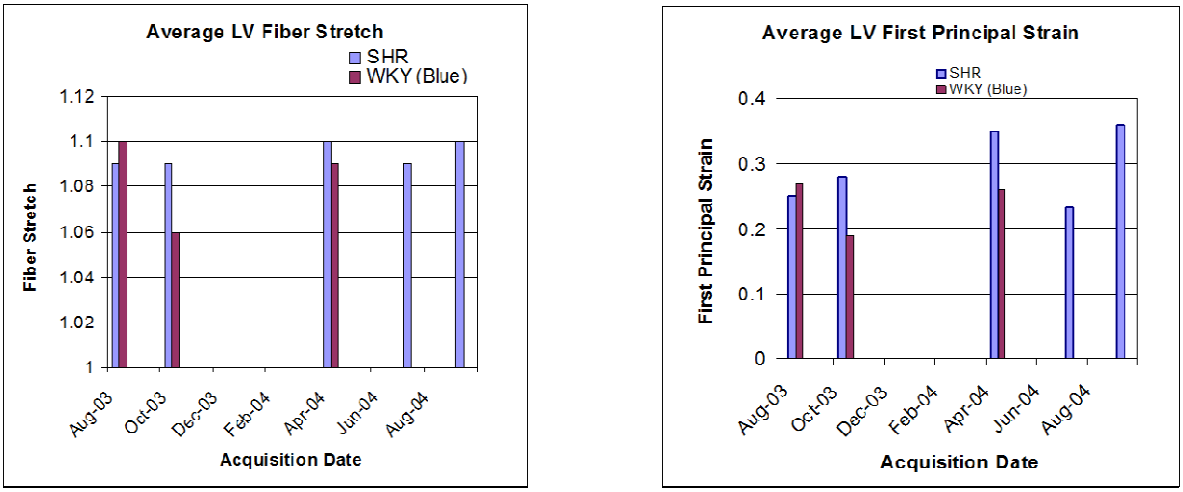

Figure 4. Average left ventricle fiber stretch and first principal Green-Lagrange strain as a function of age for one hypertensive SHR rat and one normotensive WKY (Blue) control rat. The Warping analysis could not be performed on the control rats after June, 2004 due to insufficient uptake of ^{18}FDG.

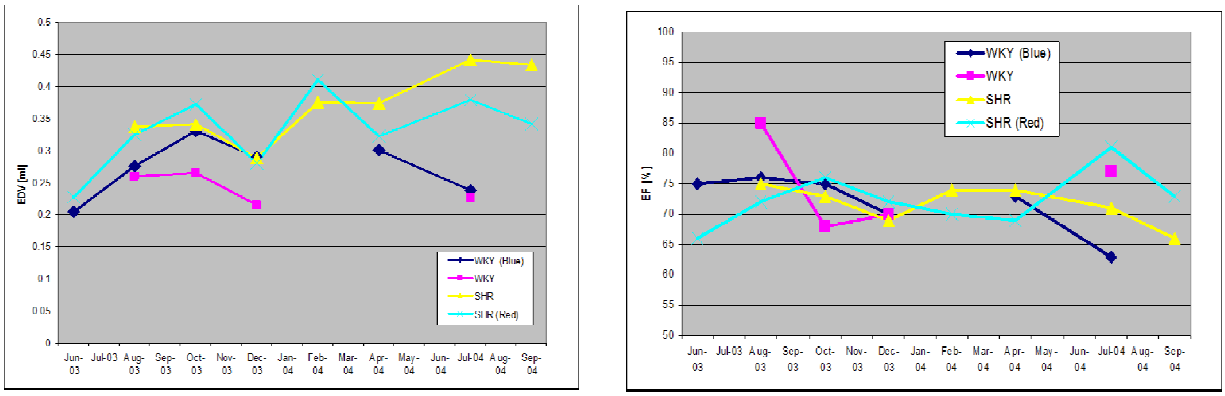

Figure 5. End diastolic volume and ejection fraction as a function of age for the two hypertensive SHR rats and two normotensive WKY rats.

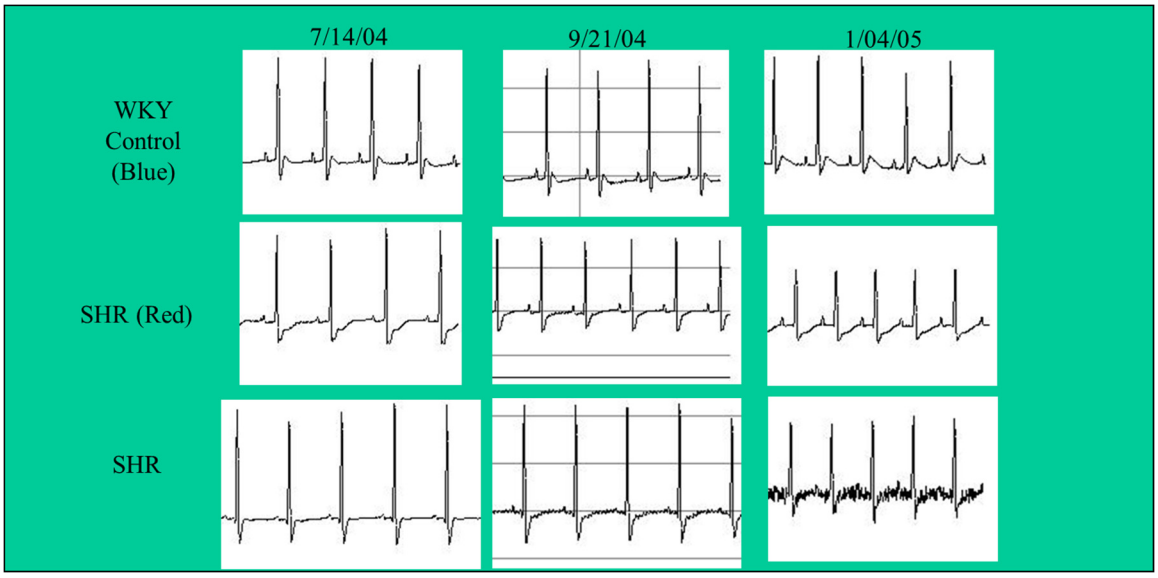

Figure 6. The ECG data provides the following discernable differences between the hypertensive rats and controls:

- A slight increase in ratio of about 10:7 on average of the QRS complex for the Controls vs. SHRs
- Slight increase of QRS interval for SHRs over that of the Controls [especially SHR (red)]
- Increased ST depression, with very slight or not noticeable T wave for SHR rats. This is in contrast to the Control ECG which has a sharp depolarization wave, as well as a noticeable T wave.

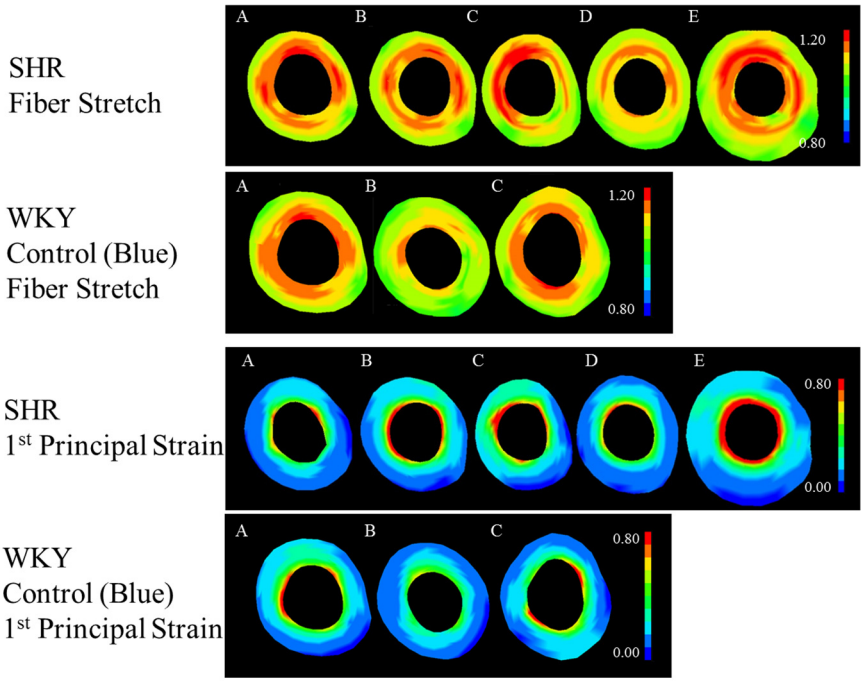

Figure 7. Temporal comparison of diastolic fiber stretch and 1st Principal strain for the SHR and WKY control (Blue). Date of scan: (A) 8/06/03; (B) 10/01/03; (C) 4/27/04; (D) 7/14/04; (E) 9/21/04.

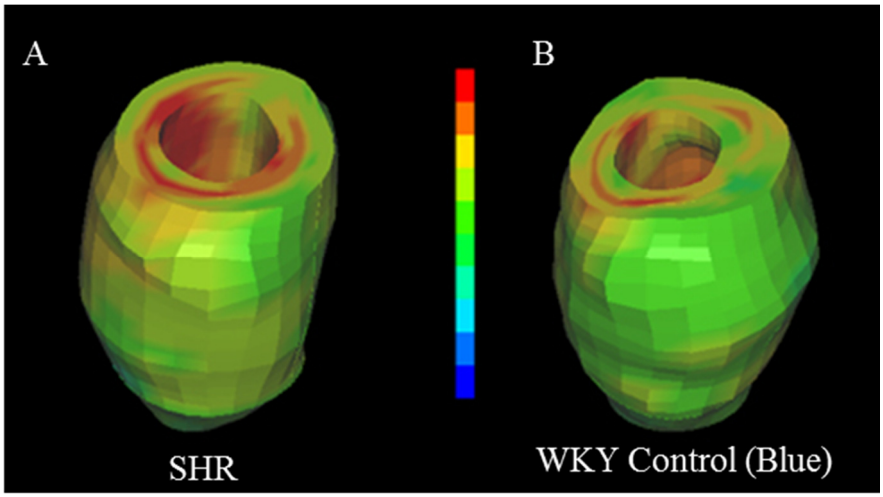

Figure 8. Comparison of diastolic fiber stretch (4/27/04 date of scan).

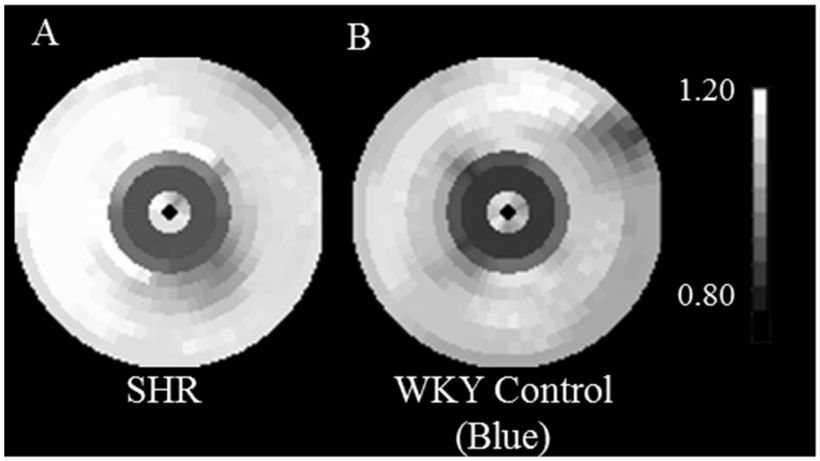

Figure 9. Bullseye plots of diastolic fiber stretch. The SHR rat shows greater anterior/lateral fiber stretch than the WKY control (Blue) (4/27/04 date of scan).

Metabolism

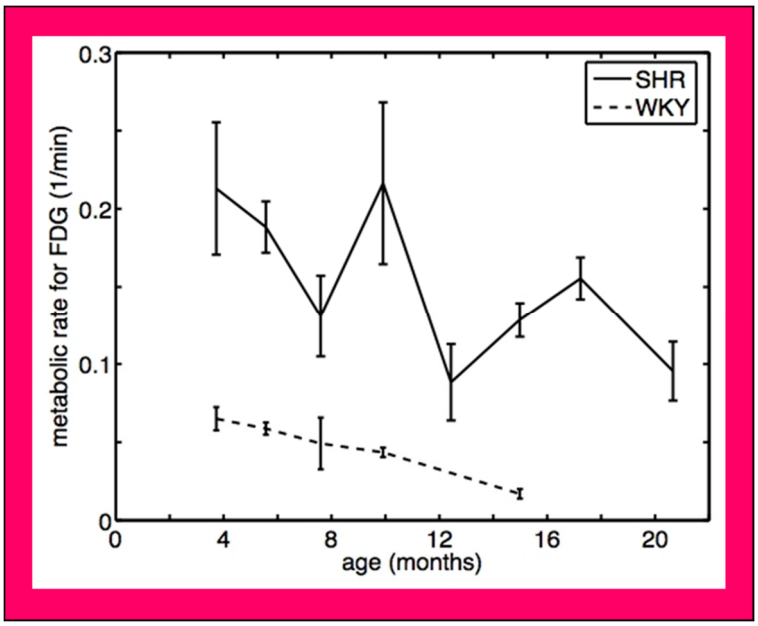

Figure 10. The metabolic rate of ^{18}FDG as a function of age for the hypertensive SHR rat and the WKY control rat. The metabolic rate is $(k_{21}k_{32})/(k_{12}+k_{32})$, calculated from the compartment model shown in Figure 3.

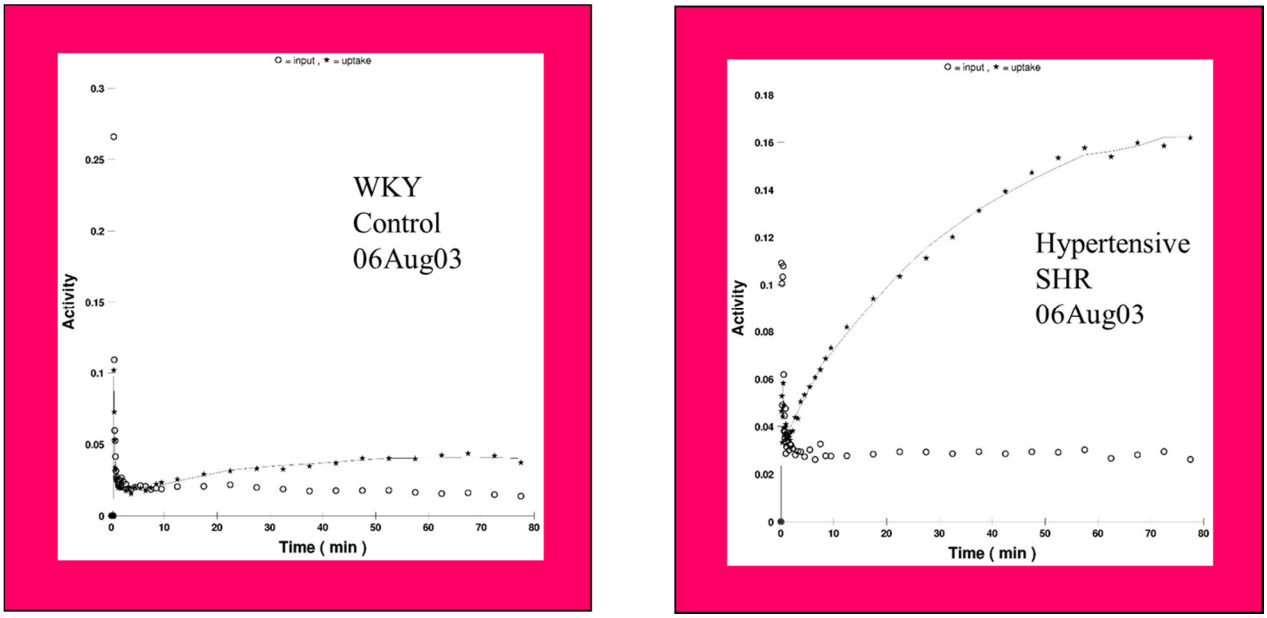

Figure 11. The fits for the time activity curves obtained on 06Aug03 for the hypertensive SHR rat and the normotensive WKY control rat. The metabolic rate of ^{18}FDG was 0.21±0.04 for the SHR and 0.065±0.007 for the WKY rat.

SUMMARY

- In the case of pressure overload there is an increased reliance on carbohydrate oxidation in an attempt to maintain contractile function.
- The results indicate that the metabolic rate of FDG decreases with the SHR rats but remains considerably higher than the normotensive WKY rats.
- The anterior/lateral free wall of the SHR rat shows a greater fiber stretch and strain than the normal control WKY (Blue) rat.
- For the control WKY rats, the ECG waveform remained mostly constant. For the SHR rats, increased ST depression may be indicative of subendocardial ischemia or infarction; widening QRS complex may be symptomatic of Right Bundle Branch Block (RBBB).

Disclaimer

This document was prepared as an account of work sponsored by the United States Government. While this document is believed to contain correct information, neither the United States Government nor any agency thereof, nor The Regents of the University of California, nor any of their employees, makes any warranty, express or implied, or assumes any legal responsibility for the accuracy, completeness, or usefulness of any information, apparatus, product, or process disclosed, or represents that its use would not infringe privately owned rights. Reference herein to any specific commercial product, process, or service by its trade name, trademark, manufacturer, or otherwise, does not necessarily constitute or imply its endorsement, recommendation, or favoring by the United States Government or any agency thereof, or The Regents of the University of California. The views and opinions of authors expressed herein do not necessarily state or reflect those of the United States Government or any agency thereof or The Regents of the University of California.

ACKNOWLEDGMENTS

We want to thank Simon Cherry, PhD for access to the microPET II at UC Davis and Kathleen Brennan, DVM and Steve Rendig for help with the animal studies. We also want to thank Thomas Ng for help with obtaining blood pressure measurements and Scott Taylor, PhD for help preparing the histology samples. This work was supported under NIH grant R01 EB00121, NSF grant BES-0134503, and DOE contract DE-AC03-76SF00098.

REFERENCES

[1] Lahiri A, Rodrigues EA, Carboni GP, Raftery EB. Effects of chronic treatment with calcium antagonists on left ventricular diastolic function in stable angina and heart failure. *Circ* **81 (suppl III)**:130-138, 1990.

[2] Germano G, Kiat H, Kavanagh PB, Moriel M, Mazzanti M, Su HT, Van Train KF, Berman DS. Automatic quantification of ejection fraction from gated myocardial perfusion SPECT. *J Nucl Med* **36**:2138-2147, 1995.

[3] Faber TL, Cooke CD, Folks RD, Vansant JP, Nichols KJ, DePuey EG, Pettigrew RI, Garcia EV. Left ventricular function and perfusion from gated SPECT perfusion images: An integrated method. *J Nucl Med* **40**:650-659, 1999.

[4] Opie LH: *The Heart: Physiology and Metabolism* Second Edition. Raven Press, New York, 1991.

[5] Taylor M, Wallhaus TR, Degrado TR, Russell DC, Stanko P, Nickles RJ. An evaluation of myocardial fatty acid and glucose uptake using PET with [^{18}F]fluoro-6-thia-heptadecanoic acid and [^{18}F]FDG in patients with congestive heart failure. *J Nucl Med* **42**:55-62, 2001.

[6] Kataoka K, Nohara R, Hosokawa R, Hirai T, Okuda K, Li-Guang C, Fujibayashi Y, Fujita M, Konishi J, Sasayama S. Myocardial lipid metabolism in compensated and advanced stages of heart failure: Evaluation by canine pacing model with BMIPP. *J Nucl Med* **42**:124-129, 2001.

[7] Katz AM. Mechanisms and abnormalities of contractility and relaxation in the failing heart. *Cardiologia* **38**:39-43, 1993.

[8] Taegtmeyer H, Golfman L, Sharma S, Razeghi P, Van Arsdall M. Linking gene expression to function: Metabolic flexibility in the normal and diseased heart. *Ann NY Acad Sci* **1015**:202-213, 2004.

[9] Young ME, Laws FA, Goodwin GW, Taegtmeyer H. Reactivation of peroxisome proliferator-activated receptor α is associated with contractile dysfunction in hypertrophied rat heart. *J Biological Chem* **276**:44390-44395, 2001.

[10] Haft JL: Cardiovascular injury induced by sympathetic catecholamines. *Prog Cardiovas Dis* **17**:73-85, 1974.

[11] Raynolds MV, Bush EW, Taft CS, Roden RA, Bristow MR. Altered gene expression of several rate-limiting enzymes in fatty acid oxidation and glycolysis in the failing human heart. *Circ* **90 (suppl 1)**:I-209, 1994.

[12] Maker BN, Ferencz RM, Hollquist JO. NIKE3D. A Nonlinear, Implicit, Three-Dimensional Finite Element Code for Solid and Structural Mechanics. Lawrence Livermore National Laboratory Technical Report, *UCRL-MA-105268,* 1990.

[13] Weiss JA, Maker BN, Govindjee S. Finite element implementation of incompressible, transversely isotropic hyperelasticity. *Computer Methods in Applied Mechanics and Engineering* **135**:107-128, 1996.

[14] Vaplon SM, Omens JH, McCulloch AD. Ventricular tissue adaptation associated with collagen deficiency in the osteogenesis imperfecta murine. Presented at 1999 Bioengineering Conference, Big Sky, Montana, June 16-20, 1999.

[15] Emery JL, Omens JH, McCulloch, AD. Biaxial mechanics of the passively overstretched left ventricle. *Am J Physiol* **272**: H2299-305, 1997.

[16] Veress AI, Weiss JA, Gullberg GT, Vince DG, Rabbitt RD. Strain measurement in coronary arteries using intravascular ultrasound and deformable images. *J Biomechanical Eng* **124**:734-741, 2003.

[17] Weiss JA, Rabbitt RD, Bowden AE. Incorporation of medical image data in finite element models to track strain in soft tissues. SPIE **3254**:477-484, 1998.

[18] Yavuz M, Fessler JA. Statistical image reconstruction methods for randoms-precorrected PET scans. *Medical Image Analysis* **2**:369-378, 1998.

[19] Qi J, Leahy RM, Cherry SR, Chatziioannou A, Farquhar TH. High resolution 3D Bayesian image reconstruction using the microPET small animal scanner. *Phys Med Biol* **43**:1001-1013, 1998.

[20] Sitek A, El Fakhri G. A generalized approach to ensuring unique solutions in factor analysis of dynamic sequences. In *2003 IEEE Nuclear Science Symposium and Medical Imaging Conference Record*, Oct. 18-23, 2004, Rome, Italy.

[21] Huesman RH, Knittel BL, Mazoyer BM, Coxson PG, Salmeron EM, Klein GJ, Reutter BW, Budinger TF. Notes on RFIT: A program for fitting compartmental models to region-of-interest dynamic emission tomographic data. Lawrence Berkeley National Laboratory Report, *LBL-37621*, 1995.